NIH Public Access
Author Manuscript
Biomacromolecules. Author manuscript; available in PMC 2011 March 8.

Published in final edited form as:
Biomacromolecules. 2010 March 8; 11(3): 648–656. doi:10.1021/bm9012293.

Photo-crosslinked $PDMS_{star}$-PEG Hydrogels: Synthesis, Characterization, and Potential Application for Tissue Engineering Scaffolds

Yaping Hou[1], **Cody A. Schoener**[1], **Katherine R. Regan**[1], **Dany Munoz-Pinto**[2], **Mariah S. Hahn**[2], and **Melissa A. Grunlan**[1,*]

[1] Department of Biomedical Engineering, Texas A&M University, College Station, TX 77843-3120

[2] Department of Chemical Engineering, Texas A&M University, College Station, TX 77843-3120

Abstract

Inorganic-organic hydrogels with tunable chemical and physical properties were prepared from methacrylated star polydimethylsiloxane ($PDMS_{star}$-MA) and diacrylated poly(ethylene glycol) (PEG-DA) for use as tissue engineering scaffolds. Eighteen compositionally unique hydrogels were prepared by photo-crosslinking varying weight ratios of PEG-DA and $PDMS_{star}$-MA of different molecular weights (M_n): PEG-DA (M_n = 3.4k and 6k g/mol) and $PDMS_{star}$-MA (M_n = 1.8k, 5k and 7k g/mol). Introduction of $PDMS_{star}$-MA caused formation of discrete PDMS-enriched microparticles dispersed within the PEG matrix. The swelling ratio, mechanical properties in tension and compression, non-specific protein adhesion, controlled introduction of bioactivity and cytotoxicity of hydrogels were studied. This library of inorganic-organic hydrogels with tunable properties provides a useful platform to study the effect of scaffold properties on cell behavior.

Keywords

poly(ethylene glycol); polydimethylsiloxane; hydrogel; scaffold

Introduction

Tissue engineering (TE) seeks to repair or replace damaged or diseased tissues and organs.[1] A three-dimensional polymeric scaffold is often used to create an environment in which living cells can attach, proliferate, differentiate, and ultimately produce a new extracellular matrix (ECM).[2–4] Synthetic polymers generally provide greater control and range of chemical and physical properties compared to natural polymers.[2, 4, 5] Synthetic hydrogels have been widely studied as tissue engineering scaffolds.[5–7] Hydrogels are hydrated polymer networks comprised of hydrophilic polymers which are crosslinked via chemical bonds or physical interactions.[8, 9] The utility of hydrogels as scaffolds is attributed to several factors, including superior biocompatibility which minimizes inflammation, thrombosis and tissue damage, as well as high diffusivity and elasticity which parallels many tissues.[5–7] Compared to thermal or redox initiated crosslink mechanisms, photo-induced free radical hydrogel crosslinking produces less heat while allowing for improved spatial and temporal control. As a result,

*mgrunlan@tamu.edu.

Supporting Information Available. FE-SEM/EDS of $C_{20}H_{80}$. This material is available free of charge via the Internet at http://pubs.acs.org.

NIH-PA Author Manuscript
NIH-PA Author Manuscript
NIH-PA Author Manuscript

NIH-PA Author Manuscript

NIH-PA Author Manuscript

NIH-PA Author Manuscript

geometrically complex scaffolds may be rapidly formed *in situ* from cells suspended in aqueous solutions of monomers or macromers and may be done so *in vivo*.[10, 11]

Photopolymerizable poly(ethylene glycol) diacrylate (PEG-DA) based hydrogels have been extensively utilized as scaffolds for the regeneration of tissues including bone,[12, 13] cartilage,[11, 14, 15] nerve,[16] and vascular tissue.[17, 18] PEG hydrogels are particularly useful for controlled studies of cell-material interactions because of their intrinsic resistance to protein absorption and cell adhesion.[19] Thus, PEG hydrogels are "biological blank slates" in which cell-material interactions may be limited to the adhesive ligands introduced.[12, 13, 20] To permit eventual replacement by the growing tissue, biodegradable PEG hydrogels have been formed by incorporation of enzymatically labile peptides[21, 22] or hydrolytically labile linear esters.[23–25]

In natural tissues, the ECM mediates critical cell function, including regeneration, via signaling cascades involving specific binding events as well as non-specific chemical and physical features.[26, 27] Thus, development of scaffolds having specific properties which guide cell behavior is critical for tissue regeneration.[28] Certain scaffold material properties have been shown to impact cell behavior.[29, 30] For instance, the chemical nature of the scaffold, in terms of bioactivity, chemical functionality, and hydrophilicity has been shown to influence cell behavior.[31–36] Physical properties such as scaffold morphology[37–39] and modulus[40–42] also affect cell behavior.

In order to guide cell behavior through cell-material interactions, scaffolds with precisely tunable chemical and physical properties are crucial. For such studies, synthetic hydrogel scaffolds with chemical and physical properties which can be finely and easily controlled are required. For PEG-DA hydrogels, crosslink density and mechanical properties may be tailored by simply varying the molecular weight and/or the concentration of PEG-DA.[43] However, since PEG-DA hydrogels are single-component systems, the ability to uncouple various material properties, such as modulus and swelling, is limited.[44] Thus, hydrogels that maintain the benefits of PEG-DA while extending the ability to tune and uncouple material properties would further enhance the ability to establish relationships between cell behavior and scaffold properties.

In this study, both the chemical and physical properties of PEG-DA hydrogels were tuned by introduction of a methacrylated star polydimethylsiloxane ($PDMS_{star}$-MA) macromonomer. PDMS is an inorganic polymer which is biocompatible, hydrophobic, exhibits excellent gas permeability, low glass transition temperature (T_g, −127 °C), and exceptional elasticity when lightly crosslinked.[45] The hydrogels reported herein are two component systems and so the average number molecular weight (M_n) and concentration of both macromonomers (i.e. PEG-DA and $PDMS_{star}$-MA) were used to tailor hydrogel properties. The chemical properties of the hydrogels were switched from purely organic PEG to inorganic-organic $PDMS_{star}$-PEG by introducing increased levels of $PDMS_{star}$-MA. In addition, the effect of hydrogel composition on physical properties, including morphology, equilibrium swelling (i.e. hydration), mechanical properties, non-specific protein adsorption, controlled introduction of bioactivity and cytotoxicity, were examined.

Experimental Section

Materials

Pt-divinyltetramethyldisiloxane complex (Karstedt's catalyst, 2 wt% in xylene), tetrakis (dimethylsiloxy)silane (tetra-SiH), and octamethylcyclotetrasiloxane (D_4) were obtained from Gelest. Allyl methacrylate, acryloyl chloride, triflic acid, 2,2-dimethyl-2-phenyl-acetophenone (DMAP), 1-vinyl-2-pyrrolidinone (NVP), triethylamine (Et_3N), $MgSO_4$, K_2CO_3, hexamethyldisilazane (HMDS), N3013 Nile Red (Nile Blue A Oxazone) and solvents were

NIH-PA Author Manuscript

NIH-PA Author Manuscript

NIH-PA Author Manuscript

obtained from Sigma Aldrich. HPLC grade toluene and CH_2Cl_2 and NMR grade $CDCl_3$ were dried over 4Å molecular sieves. Poly(ethylene glycol) (PEG) [PEG-6000; MW = 5000–7000 g/mol and PEG-3400; MW = 3000–3700 g/mol per manufacturer's specifications] were obtained from BioChemika. The M_n of PEG-3400 (3274 g/mol) and PEG -6000 (5881 g/mol) were back-calculated from ^{1}H NMR end-group analysis of the corresponding diacrylated products (**L** and **H**, respectively). Phosphate buffered solution (PBS, pH = 7.4, without calcium and magnesium), HEPES, Dulbecco's Modified Eagle Medium (DMEM), fetal bovine serum (FBS), and PSA solution (10 U/mL penicillin, 10 g/L streptomycin, and 10 g/L amphotericin) were obtained from Mediatech. Peptide RGDS was obtained from American Peptide. Acryloyl PEG-*N*-hydroxysuccinimide (acryloyl-PEG-NHS, 3.4 kDa) was obtained from Nextar. Mouse smooth muscle precursor cells (10T1/2) were obtained from American Type Culture Collection (ATCC).

Synthesis of Photo-crosslinkable Macromonomers

All reactions were run under a N_2 atmosphere with a Teflon-covered stir bar to agitate the reaction mixture. $PDMS_{star}$-MA (**A–C**) were prepared in two synthetic steps (Figure 1). First, silane-terminated star polydimethylsiloxanes ($PDMS_{star}SiH$) (**a–c**) were prepared by the acid-catalyzed equilibration of octamethylcyclotetrasiloxane (D_4) with tetrakis(dimethylsiloxy) silane (tetra-SiH).[46] These reagents were combined in a 200 mL round bottom (rb) flask equipped with a rubber septum and triflic acid added via syringe. The mixture was allowed to stir for 16 h at room temperature (RT) and excess HMDS added to neutralize the mixture. The polymer mixture was precipitated three times in toluene/MeOH and the isolated polymer dried under reduced pressure. In the second step, Pt-catalyzed hydrosilylation of **a–c** each with allyl methacrylate yielded **A–C**, respectively.[47] In a 250 mL 3-neck rb flask equipped with an addition funnel and rubber septum, **a–c** were each combined with ~30 mL toluene and the mixture heated to 45 °C. After dropwise addition of allyl methacrylate, the mixture was heated to 90 °C and Karstedt's catalyst added via syringe. The progress of the reaction was monitored with IR spectroscopy by the disappearance of the Si-H (~2125 cm^{-1}) absorbance. After ~12 h, an aliquot of the reaction solution was evaporated on a NaCl plate and the IR spectrum obtained. In case of an incomplete reaction, additional Karstedt's catalyst (50% of original volume) was added and the reaction continued for another ~6 h before checking the IR spectrum. This cycle was repeated until no Si-H absorbance was observed in the IR spectrum. Typically, no additional Kartstedt's catalyst was required to complete the reaction. After removal of volatiles under reduced pressure, the catalyst was removed from the residue via flash column chromatography on silica gel with hexanes:ethyl acetate (2:1 vol:vol) and volatiles removed under reduced pressure.

PEG-DA (**L, H**) were prepared by acrylating the terminal hydroxyl groups of linear PEG [3.4k g/mol ("low" M_n) and 6k g/mol ("high" M_n), respectively].[48] Dry PEG was dissolved in CH_2Cl_2 in a 300 mL rb flask equipped with a rubber septum. Et_3N and acryloyl chloride were sequentially added slowly via syringe. The reaction mixture was allowed to stir at RT overnight. The mixture was transferred to a separatory funnel and washed with 2M K_2CO_3. After allowing the layers to separate overnight, the organic layer was isolated, dried with $MgSO_4$ and gravity filtered. The filtrate was precipitated in diethyl ether, vacuum filtered, washed with diethyl ether and dried under vacuum (30 in. Hg).

Synthesis of $PDMS_{star}$-SiH (a)

D_4 (30 g, 101.4 mmol), tetra-SiH (7.8 g, 23.8 mmol), triflic acid (60 μL), and HMDS (0.15 g, 0.93 mmol) were reacted as above. In this way, **a** (23.3 g, 62% yield) was obtained as a colorless liquid, M_n/M_w= 1,700/2,700 g/mol, PDI = 1.6. ^{1}H NMR (δ, ppm): 0.025–0.19 (bm, 231H, SiCH_3), 4.7 (m, 4H, Si*H*). IR (ν): 2130 cm^{-1} (Si-H).

NIH-PA Author Manuscript

NIH-PA Author Manuscript

NIH-PA Author Manuscript

Synthesis of $PDMS_{star}$-SiH (b)

D_4 (29.9 g, 101.0 mmol), tetra-SiH (1.7 g, 5.2 mmol), triflic acid (60 μL), and HMDS (0.15 g, 0.93 mmol) were reacted as above. In this way, **b** (23.7 g, 75% yield) was obtained as a colorless liquid, M_n/M_w= 4,800/11,200 g/mol, PDI = 2.3. ^{1}H NMR (δ, ppm): 0.010–0.175 (bm, 1038H, Si*CH*$_3$), 4.7 (m, 4H, Si*H*). IR (ν): 2130 cm^{-1} (Si-H).

Synthesis of $PDMS_{star}$-SiH (c)

D_4 (29.9 g, 101.0 mmol), tetra-SiH (1.1 g, 3.4 mmol), triflic acid (60 μL), and HMDS (0.15 g, 0.93 mmol) were reacted as above. In this way, **c** (24.4 g, 79% yield) was obtained as a colorless liquid, M_n/M_w= 6,800/17,700 g/mol, PDI= 2.6. ^{1}H NMR (δ, ppm): 0.064–0.113 (bm, 1114H, Si*CH*$_3$), 4.7 (m, 4H, Si*H*). IR (ν): 2130 cm $^{-1}$ (Si-H).

Synthesis of $PDMS_{star}$-MA (A)

a (1.5 g, 0.88 mmol), allyl methacrylate (0.42 g, 3.33 mmol), toluene (3 mL), and Karstedt's catalyst (20 μL) were reacted as above. In this way, **A** (1.1 g, 57% yield) was obtained as a colorless liquid, M_n/M_w= 2,050/4,800 g/mol, PDI = 2.3. ^{1}H NMR (δ, ppm): 0.045–0.127 (bm, 282H, Si*CH*$_3$), 0.306 (m, 9H, Si*CH*$_3$), 0.563 (m, 8H, -Si*CH*$_2$CH$_2$CH$_2$, 1.69 (m, 8H, -SiCH$_2$*CH*$_2$CH$_2$), 1.93 (s, 12H, C(CH$_2$)*CH*$_3$), 4.10 (m, 8H, -SiCH$_2$CH$_2$*CH*$_2$), 5.58 (m, 4H, -C(*CH*$_2$)CH$_3$), 6.11 (m, 4H, -C(*CH*$_2$)CH$_3$). IR (ν): no Si-H peak. Slightly less than 4 equivalence of allyl methacrylate was added to obtain **A** without trace allyl methacrylate. This stoichiometric variation may be due to the error associated in GPC determination of M_n of **a**.

Synthesis of $PDMS_{star}$-MA (B)

b (20.04 g, 4.1 mmol), allyl methacrylate (2.3 g, 18.1 mmol), toluene (35 mL), and Karstedt's catalyst (100 μL) were reacted as above. In this way, **B** (20.7 g, 97% yield) was obtained as a colorless liquid, M_n/M_w = 5,000/14,450 g/mol, PDI = 2.9. ^{1}H NMR (δ, ppm): 0.007–0.204 (bm, 1670H, Si*CH*$_3$), 0.293 (m, 9H, Si*CH*$_3$), 0.587 (m, 8H, -Si*CH*$_2$CH$_2$CH$_2$), 1.70 (m, 8H, -SiCH$_2$*CH*$_2$CH$_2$), 1.95 (s, 12H, -C(CH$_2$)*CH*$_3$), 4.11 (m, 8H, -SiCH$_2$CH$_2$*CH*$_2$), 5.60 (s, 4H, -C(*CH*$_2$)CH$_3$), 6.13 (s, 4H, -C(*CH*$_2$)CH$_3$). IR (ν): no Si-H peak.

Synthesis of $PDMS_{star}$-MA (C)

c (20.0 g, 2.9 mmol), allyl methacrylate (1.6 g, 12.7 mmol), toluene (35 mL), and Karstedt's catalyst (100 μL) were reacted as above. In this way, **C** (10.4 g, 48% yield) was obtained as a colorless liquid, M_n/M_w= 7,000/23,400 g/mol, PDI = 3.3. ^{1}H NMR (δ, ppm): 0.004–0.266 (bm, 1746H, Si*CH*$_3$), 0.571 (m, 8H, -SiCH$_2$*CH*$_2$CH$_2$), 1.69 (m, 8H, -SiCH$_2$*CH*$_2$CH$_2$), 1.95 (s, 12H, -C(CH$_2$)*CH*$_3$), 4.10 (m, 8H, -SiCH$_2$CH$_2$*CH*$_2$), 5.58 (s, 4H, -C(*CH*$_2$)CH$_3$), 6.15 (s, 4H, -C(*CH*$_2$)CH$_3$). IR (ν): no Si-H peak.

Synthesis of PEG-DA (L)

PEG-3350 (23.5 g, 7.0 mmol), Et_3N (1.95 mL, 14.0 mmol) and acryloyl chloride (2.27 mL, 28.0 mmol) were reacted as above. In this way, **L** (18.3 g, 76% yield) was obtained. ^{1}H NMR (δ, ppm): 3.62 (s, 296H, -O*CH*$_2$*CH*$_2$), 5.81 (dd, 2H, *J* = 10.2 and 1.5 Hz, -CH=C*H*$_2$), 6.12 (dd, 2H, *J* = 17.3 and 10.5 Hz, -C*H*=CH$_2$), 6.40 (dd, 2H, *J* = 17.3 and 1.5 Hz, -CH=C*H*$_2$). By ^{1}H NMR end-group analysis, M_n of **L** was determined to be 3382 g/mol (~3400 g/mol).

Synthesis of PEG-DA (H)

PEG-6000 (24.0 g, 4.0 mmol), Et_3N (1.12 mL, 8.0 mmol) and acryloyl chloride (1.3 mL, 16.0 mmol) were reacted as above. In this way, **H** (17.9 g, 75% yield) was obtained. ^{1}H NMR (δ, ppm): 3.61 (s, 533H, -O*CH*$_2$*CH*$_2$), 5.81 (dd, 2H, *J* = 10.2 and 1.5 Hz, -CH=C*H*$_2$), 6.12 (dd,

NIH-PA Author Manuscript

NIH-PA Author Manuscript

NIH-PA Author Manuscript

2H, *J* = 17.1 and 10.5 Hz, -C*H*=CH_2), 6.39 (dd, 2H, *J* = 17.3 and 1.5 Hz, -CH=C*H*$_2$). By ^{1}H NMR end-group analysis, M_n of **H** was determined to be 5989 g/mol (~6000 g/mol).

Hydrogel Preparation

Hydrogels were prepared by the photopolymerization of aqueous mixtures of $PDMS_{star}$-MA **(A–C)** and PEG-DA **(L, H)** macromonoomers. Aqueous precursor solutions were prepared at 10 wt%. 10 μL of photoinitiator solution (30 wt% solution of DMAP in NVP) was added per one mL of the aqueous solution. The $PDMS_{star}$-MA and photoinitiator solution were sequentially added to an aqueous solution of PEG-DA and vortexed for 1 min after each component was added. The resulting emulsions prepared with **A–C** were hazy but did not separate into layers. These were immediately used to form hydrogels. Hydrogels were prepared with the following wt% ratios of **A**, **B**, or **C** to **L** or **H**: 0:100, 1:99, 10:90 and 20:80 (Table 1).

Planar hydrogel sheets (1.0 or 1.5 mm thick) were prepared by pipetting the precursor solution between two clamped microscope slides (75 × 50 or 50 × 40 mm) separated by polycarbonate spacers and exposing the mold to longwave UV light (UV-Transilluminator, 6 mW/cm^2, 365 nm) for 80 sec. After removal from the mold, the hydrogel sheet was rinsed with DI water and then soaked in PBS for 2 days with daily PBS changes to remove catalyst impurities. A weight loss due to unreacted sol was not observed. Hydrogel sheets prepared in this way were used for morphological, swelling, compression, protein adhesion, and cytotoxicity tests.

For tensile tests, hydrogels were prepared with a “ring” geometry. First, hydrogels were prepared in a hollow tube geometry with a double walled tubular mold composed of an inner glass mandrel (diameter = 3 mm) and an outer glass cylinder (diameter = 7.5 mm). The tubular mold was filled with a precursor solution and cured as above but with constant rotation such that each surface point of the mold received equal UV intensity and exposure time. The hydrogel tube was removed from the mold and similarly purified as above by rinsing and soaking in PBS. Ring specimens were obtained but cutting ~3 mm wide pieces from the central portion of the hydrogel tube.

Polymer Characterization

NMR

^{1}H spectra were obtained on a Mercury 300 300-MHz spectrometer operating in the Fourier transform mode. Five percent (w/v) $CDCl_3$ solutions were used.

IR Spectroscopy

IR spectra of neat liquids on NaCl plates were recorded using a Bruker TENSOR 27 Fourier transform infrared spectrometer.

Gel Permeation Chromatography

Gel permeation chromatography (GPC) analysis was performed on a Viscotek GPC system equipped with three detectors in series: refractive index (RI), right angle laser light scattering (RALLS), and viscometer (VP). The ViscoGEL HR-Series (7.8mm × 30 cm) column packed with divinylbenzene crosslinked polystyrene was maintained at 25°C in a column oven. The eluting solvent was HPLC grade toluene at a flow rate of 1.0 mL/min. The detectors were calibrated with a polystyrene narrow standard with the following parameters: M_w (115,000 g/mol), polydispersity (1.01), intrinsic viscosity (0.519 dL/g), and dn/dc (0.185 mL/g). Data analysis was performed with Viscotek OmniSec software (Version 4.0).

NIH-PA Author Manuscript

NIH-PA Author Manuscript

NIH-PA Author Manuscript

Hydrogel Characterization

Morphological Characterization

For a given hydrogel, a disc (8 mm diameter, 1.5 mm thickness) was punched from a hydrogel sheet with a die. A Nile Red solution was prepared as follows: 75 μL of a Nile Red solution (20 mg per mL of methanol) was dissolved in 8 mL of double distilled water (DDW) and combined with 120 mL of PBS. Each hydrogel disc was sequentially soaked for 24 h each in 60 mL of the aforementioned Nile Red solution and 60 mL of PBS. With each disc placed on a glass microscope slide and DDW dropped onto the disc to maintain hydration, images were captured with confocal laser scanning microscopy (CLSM) using a Leica TCS SP5 confocal microscope (Leica Microsystems, Bannockburn, IL; excitation filter of 488 nm and emission filter 490–570 nm. Images were acquired in 3-μm steps from the top to the bottom of the hydrogel and the first 100 stack reconstructed to create a 3D images using Osirix software. Images were assigned green color to improve contrast.

Energy Dispersive X-Ray Spectrometry (EDS)

Identification of elemental compositions of specific regions of a hydrogel was performed with a field emission scanning electron microscope and energy dispersive X-ray spectrometer (FE-SEM/EDS) (FEI Quanta 600). The hydrogel was crosslinked with ruthenium vapor, plunged into liquid nitrogen and sequentially soaked in HMDS and ethanol. The samples were sputter coated with Pt/Pd at the surface with 4 nm thickness.

Equilibrium Swelling

For a given hydrogel, three hydrogel discs (13 mm diameter, 1.5 mm thickness) were punched from a single hydrogel sheet with a die. Hydrogel equilibrium swelling ratio is defined as: s*welling ratio* = $(W_s - W_d)/W_d$, where W_s is the weight of the water-swollen hydrogel at a certain temperature and W_d is the weight of the vacuum dried hydrogel (30 in. Hg, 60 °C, 24 h). Each disc was sealed inside a vial containing 20 mL PBS, immersed in a temperature controlled water bath for 24 h at 25 °C, removed, blotted with filter paper to remove surface water, and weighed (W_s).

Dynamic Mechanical Analysis (DMA)

DMA of hydrogels were measured in the compression mode with a dynamic mechanical analyzer (TA Instruments Q800) equipped with parallel-plate compression clamp with a diameter of 40 mm (bottom) and 15 mm (top). Swollen hydrogel discs of constant dimension (13 mm diameter, 1.5 mm thickness) were punched from a hydrogel sheet and clamped between the parallel plates. Silicone oil was then placed around the exposed edges of the hydrogel to prevent dehydration. The samples were tested in a multi-frequency-strain mode (1 to 18 Hz). Results reported are based on the average of five individual specimens.

Tensile Tests

Tensile tests of hydrogels ring specimens were measured on a TA Instruments DMA Q800 operating in the tension mode. Specimens with a ring geometry were prepared by cutting a portion from a hydrogel tube produced from the double wall tubular mold (ID = 3 mm, OD = 7.5 mm). Individual rings (~3 mm width) were cut from the central portion of the appropriate hydrogel tube using a clean razor blade and sample dimensions measured with an electronic caliper. Each hydrogel ring was blotted with filter paper and loaded onto custom aluminum bars gripped directly into DMA tension clamps so that the upper and lower bars were located inside the ring. Samples were subjected to a constant strain (1 mm/min) until they broke at the center of one side of the ring. Stress was calculated from the measured force divided by the cross-sectional area of two rectangles with sides equal to the width and wall thickness of the

NIH-PA Author Manuscript

NIH-PA Author Manuscript

NIH-PA Author Manuscript

ring. The gauge length corresponded to the outer diameter of the ring less the wall thickness. The following parameters were determined: (1) tensile modulus, (2) ultimate tensile strength (UTS), and (3) % strain at break. The tensile modulus was obtained from the slope of the linear part of the stress-strain curve. The UTS represents the maximum stress prior to failure. Strain was calculated from the measured displacement divided by the gauge length. Results reported are the average result of three specimens cut from central portion of the same hydrogel tube.

Protein Adhesion

The adhesion of Alexa Fluor 555 dye conjugate of bovine serum albumin (AF-555 BSA; MW = 66 kDa; Molecular Probes, Inc.) onto hydrogels was studied by fluorescence microscopy. For a given hydrogel, three hydrogel discs (14.5 mm diameter, 1.5 mm thickness) were punched from a single hydrogel sheet and placed in PBS (15 min) to ensure hydration. Immediately prior to transferring to a 24 well plate, discs were gently blotted with filter paper to remove surface water. Of the three discs, two discs were each placed in wells containing 1.5 mL BSA (0.1 mg/mL) and the third disc placed in a well containing 1.5 mL of PBS. Hydrogel discs were maintained in the dark at RT for 3 h. Next, from both the top and bottom surfaces of the discs, the BSA solution was carefully removed via aspiration and both sides of the disc rinsed with fresh PBS 3 times for 1 hour each time to permit the diffusion of unadsorbed protein out of the hydrogels before imaging. No measurable internal fluorescence signal was detected following rinsing. Each of these discs was returned to a well containing 1.5 mL of fresh PBS for imaging.

A Zeiss Axiovert 200 optical microscope equipped with a A-Plan 5x objective, Axiocam HRC Rev. 2), and filter cube (excitation filter of 546 ± 12 nm [band pass] and emission filter 575–640 nm [band pass]) was used to obtain fluorescent images on 3 randomly selected regions each hydrogel surface. The fluorescent light source was permitted to warm up for 30 min prior to image capture. Linear operation of the camera was ensured and constant exposure time used during the image collection to permit quantitative analyses of the observed fluorescent signals. The fluorescence microscopy images were analyzed using the histogram function of PhotoShop, which yielded the mean and standard deviation of the fluorescence intensity within a given image. For a given hydrogel composition, the average fluorescence intensity of the two discs exposed to AF-555 BSA was subtracted from that of the disc maintained only in PBS to ensure correction for of any fluorescence signal from the material itself. The background-corrected fluorescence intensities for each hydrogel were then used to quantify AF-555 BSA levels adsorbed by comparison against a calibration curve constructed from the measured fluorescence intensities of AF-555 BSA standard solutions. Standard solutions were prepared at 0, 0.005, 0.01, 0.02, and 0.04 mg/mL AF-555 BSA in PBS and each placed into an individual well containing a pure PEG hydrogel discs (**H control**).

Controlled Introduction of Cell Adhesion and Spreading (Bioactivtiy)

Hydrogels **H control** and $\mathbf{A_{10}H_{90}}$ were prepared with and without 1 μmol/mL of acrylate-derivatized cell-adhesive peptide RGDS. Acryloyl-PEG-RGDS was prepared by reacting acryloyl PEG-*N*-hydroxysuccinimide (acryloyl-PEG-NHS, 3.4 kDa) with RGDS.[18] Planar hydrogel sheets (50 × 40 × 1.0 mm) were photopolymerized as above and then immersed in DMEM supplemented with 10% FBS overnight. 10T½ SM progenitor cells were seeded onto each hydrogel surface at ~10,000 cells/cm^2. Cell adhesion and spreading was examined at 24 h using a bright field microscope (Zeiss Axiovert).

Cytotoxicity

The cytotoxicity of hydrogels was assessed by measuring lactate dehydrogenase (LDH) levels released by 10T½ SM progenitor cells at 24 and 72 h post-photoencapsulation. Cells were suspended (2×10^6 cells/mL) in sterile-filtered hydrogel precursor solutions prepared with HEPES buffered saline (HBS; 10 mM HEPES, 150 mM NaCl, pH = 7.4) to which was added

NIH-PA Author Manuscript

NIH-PA Author Manuscript

NIH-PA Author Manuscript

acryloyl-PEG-RGDS (1 μmol/mL). Hydrogel discs (8 per composition) were formed in the wells of a 48 well plate by the addition of 110 μL precursor solution per well and exposure to longwave UV light (UV-Transilluminator, 6 mW/cm^2, 365 nm) for 2 min. The resulting cell-containing hydrogels discs were maintained or 1 h at 37 °C with 5% CO_2 in DMEM supplemented with 10% v/v heat-inactivated FBS and 1% v/v PSA solution. After transferring to a well of a 24 well plate, each disc was maintained in 500 μL of supplemented. At 24 h post-encapsulation, the media surrounding 4 of the 8 hydrogels was collected for LDH measures. The corresponding gels were digested in 0.1 N NaOH for 72 h at 37 °C and DNA levels were measured using a PicoGreen assay (Invitrogen). The same process was repeated on the remaining hydrogels at 72 h. For both time points, the average LDH activity was normalized by the DNA amount in the sample.

Non-cytotoxicity of select hydrogels was further assessed by measuring the viability of 10T½ SM progenitor cells at 24 and 72 h post-encapsulation with a Live-Dead assay (Invitrogen). Cells were suspended (1×10^6 cells/mL) in the PBS-based precursor solutions of **H control** and $\mathbf{A_{10}H_{90}}$. Planar hydrogel sheets (50 × 40 × 1.0 mm) were photopolymerized as above. Longwave UV light at similar intensities and exposure times has been shown to cause minimal cell death.[49–51] The resulting cell-containing hydrogels were maintained in DMEM supplemented with 10% heat-inactivated fetal bovine serum (FBS). Live-Dead staining was conducted at 24 and 72 h and images captured using a fluorescence microscope (Live stained: excitation filter 488 nm; Dead stained: excitation filter 546 nm).

Results and Discussion

Synthesis of $PDMS_{star}$-MA (A–C)

Acid-catalyzed equilibration is useful to convert cyclosiloxanes and a suitable disiloxane to linear polymer.[52] Here, Si-H-terminated star polydimethylsiloxanes ($PDMS_{star}$SiH, **a–c**) were prepared by acid-catalyzed equilibration of D_4 with tetra-SiH.[46] The molecular weight was controlled by the ratio of D_4 and tetra-SiH. Because equilibration reactions generate a mixture of linear and cyclic species, the resulting mixture was precipitated to isolate the higher molecular weight materials. The lack of cyclic materials is confirmed by GPC of **a–c.** Si-H terminal groups of **a–c** were subsequently converted to photo-sensitive methacrylate groups by Pt-catalyzed hydrosilylation of each with allyl methacrylate to yield **A–C**, respectively.[47] **A–C** exhibited a slight increase in M_w by GPC versus the corresponding **a–c** due to an apparent small amount of crosslinking, despite our efforts to minimize exposure of **A–C** to light and to promptly use in hydrogel fabrication and characterization. The chemical reaction was confirmed by the disappearance of the Si-H peak (~ 4.5 ppm) in the ^{1}H NMR spectra and Si-H absorbance (~2125 cm^{-1}) in the FT- IR spectra of **A–C**.

Hydrogel Morphology and Chemical Composition

It is known that hydrogel morphology impacts cell behavior by changing cell alignment, proximity, and cell-cell interactions.[38, 39] The morphology of PEG-DA hydrogels cannot be visualized using techniques such as scanning electron microscopy (SEM).[53] Instead, CLSM was used herein to image hydrogels which were treated with a hydrophobic dye (Nile Red) to stain PDMS-enriched regions and while maintaining hydrogel hydration. Because of the water-insolubility of PDMS, aqueous precursor solutions prepared with **A–C** were visibly hazy but did not separate into layers. Thus, photochemical cure effectively trapped the liquid microphase separation in the resulting hydrogel. This is in contrast to our previous work in which in which discrete PDMS colloidal nanoparticles were embedded within a thermoresponsive PNIPAAm hydrogel matrix during photocure.[54] In this present study, $PDMS_{star}$ polymers formed microparticles *in situ* due to the insolubility of $PDMS_{star}$ in the PEG/water solution. The CLSM images revealed that the morphology of the $PDMS_{star}$-PEG hydrogels was heterogeneous and

NIH-PA Author Manuscript

NIH-PA Author Manuscript

NIH-PA Author Manuscript

consisted of stained PDMS-enriched microparticles surrounded by a PEG-enriched matrix (Figure 2). Some staining occurred for the **L control** and **H control** due to the hydrophobic photoinitiator. FE-SEM/EDS confirmed the presence of silicon (Si) in the microparticles and its absence in the surrounding matrix (Figure S1 of the Supporting Information). Although the general morphological features of $PDMS_{star}$-PEG hydrogels were maintained, the concentration of microparticles increased with higher levels of $PDMS_{star}$-MA (**A–C**). The chemical nature of the hydrogels was also systematically changed from a purely organic to increasingly inorganic with higher levels of $PDMS_{star}$-MA (**A–C**). These discrete PDMS-enriched microparticles are expected to have an impact on cell behavior.[35, 36, 55]

Hydrogel Hydration and Mechanical Properties

Both hydration and mechanical properties of hydrogel scaffolds influence cell behavior.[40, 41] These properties are coupled in PEG-DA and other hydrogels in that the degree of hydrogel swelling is directly related to its mechanical properties and hydrogels become more rigid and stronger with decreased water content.[56] It is therefore critical to maintain hydrogel hydration during mechanical tests to achieve accurate results.[54] Tensile testing of flat, rectangular hydrogel specimens with ends secured in tension grips is often complicated by sample slippage from or breakage at the grip. Thus, specimens with a ring geometry were employed to minimize slippage/breakage for improved accuracy.[18] Ring specimens also allowed their rapid mounting on tensile bars so that testing was completed before significant water loss. During dynamic compression tests, silicone oil was placed around the hydrogel disc specimen sandwiched between two compression clamps to inhibit water loss.

Hydrogel swelling and mechanical properties are summarized in Table 2 and Figures 3–5. Hydrogels based on **H** (PEG-DA, 6k g/mol) exhibited higher swelling than that of hydrogels based on **L** (PEG-DA, 3.4k g/mol) because of the formers lower crosslink density. However, for a given hydrogel series based on **L** or **H**, the swelling ratios of $PDMS_{star}$-PEG hydrogels were not substantially different from one another or the corresponding pure PEG-DA hydrogel (**L** and **H controls**), particularly for those based on **H**. The lack of change in hydration with incorporation of **A–C** may perhaps arise from the resulting PDMS-enriched microparticles expanding the hydrogel network and thus off-setting hydrophobic contributions (Figure 2). For hydrogels based on **L**, tensile strength generally decreased with higher levels of $PDMS_{star}$-MA (**A–C**) although the M_n of **A–C** did not have a significant impact. The percent elongation at break values were generally somewhat higher than the **L control**. For hydrogels based on **H**, tensile strength values were statistically similar to the **H control** except for $\mathbf{c_{10}H_{90}}$. The percent elongation at break values were also generally somewhat higher than the **H control**.

For hydrogels based on **L**, increased levels of $PDMS_{star}$-MA (**A–C**) systematically decreased tensile modulus (Figure 3). A similar but less substantial decrease in tensile modulus was observed for hydrogels based on **H** (Figure 4). Although the weight percent of **A–C** impacted tensile modulus of $PDMS_{star}$-PEO hydrogels, the M_n of **A–C** did not. The dynamic storage modulus (G′) of select hydrogels was also measured in compression as a function of frequency (Figure 5). Based on the tensile test results, the hydrogels with 1 wt% **A–C** showed characteristics intermediate of the corresponding pure PEG-DA hydrogel and those containing 10 wt% **A–C**. Therefore, compression tests were not conducted on hydrogel compositions with 1 wt% **A–C** due to the limited additional information that would be obtained. Over the low strain conditions examined, G′ values exhibited values similar to the corresponding tensile modulus and likewise generally decreased with higher levels of **A–C**. The PDMS particles, although they do not significantly alter swelling, apparently change the manner in which the surrounding PEG-DA hydrogel network deforms under applied stress. Thus, these $PDMS_{star}$-PEO hydrogels are particularly useful to examine scaffold mechanical properties on cell behavior as modulus may be tuned independent of swelling.

NIH-PA Author Manuscript

NIH-PA Author Manuscript

NIH-PA Author Manuscript

Non-specific Protein Adhesion

Proteins which are non-specifically adsorbed from serum or plasma as well as specifically introduced to the scaffold are known to alter cell behavior.[31, 57] Thus, to study cell behavior in response to specific, isolated scaffold properties, the protein resistant nature of PEG-DA hydrogels must be maintained. The adhesion of BSA to $PDMS_{star}$-PEG hydrogels was compared to that of the corresponding. PEG-DA hydrogels (**L** and **H controls**) (Table 2). For $PDMS_{star}$-PEG hydrogels based on **L,** BSA adsorption generally increased with increased levels of $PDMS_{star}$-MA (**A–C**). For $PDMS_{star}$-PEG hydrogels based on **H,** BSA adsorption did not vary significantly. However, for all $PDMS_{star}$-PEG hydrogels, protein adsorption levels were within the range reported for PEG-DA hydrogels.[58] It has been previously shown that BSA adsorption onto PEG-DA hydrogels is linked to its hydrophilicity.[58] Thus, despite the presence of PDMS which is highly adhesive to proteins due to its hydrophobicity,[59] the BSA adsorption onto $PDMS_{star}$-PEG hydrogels was generally not dramatically different versus PEG-DA hydrogels perhaps due to their similar hydration (swelling).

Controlled Introduction of Cell Adhesion and Spreading (Bioactivity)

The intrinsic resistance of PEG hydrogels to adsorption of bioactive serum proteins renders them “biological blank slates” because cells cannot effectively adhere and spread on synthetic gels in the absence of adsorbed proteins.[19] As a result, defined levels of cell adhesion may be introduced by covalently incorporating acrylate-derivatized cell adhesive peptide RGDS into PEG hydrogels.[12, 13, 20] Low levels of RGDS, as used here, have been observed to cause only a minimal change in hydrogel swelling.[44] It is essential that these $PDMS_{star}$-PEG hydrogels maintain this useful property of PEG hydrogels for controlled studies of cell-material interactions. As discussed above, the non-specific protein adhesion of $PDMS_{star}$-PEG hydrogels increased somewhat with increased levels of $PDMS_{star}$-MA (**A–C**) compared to the pure PEG-DA hydrogel. To confirm that these adsorbed levels are still below the threshold needed to permit cell adhesion and spreading, **H control** and $\mathbf{A_{10}H_{90}}$ hydrogels were prepared with and without 1 μmol/mL of acrylate-derivatized RGDS. In the absence of RGDS, cells similarly did not adhere and spread on both the pure PEG hydrogel (**H control**) and $PDMS_{star}$-PEG hydrogels ($\mathbf{A_{10}H_{90}}$) (Figure 6). However, modification of the $PDMS_{star}$-PEG hydrogel with RGDS produced cell adhesion and spreading. Thus, the $PDMS_{star}$-PEG scaffolds appear to permit the controlled introduction of bioactivity as observed for pure PEG hydrogels.

Cytotoxicity

Low cytotoxicity of $PDMS_{star}$-PEG hydrogels is critical for their utility as tissue engineering scaffolds. To assess the cytocompatibility of $PDMS_{star}$-PEG gels, LDH activity assays were conducted on hydrogels based on **H** and **C** (Figure 7). LDH is a soluble cytosolic enzyme that is released into the culture medium following membrane damage due to apoptosis or necrosis.[60] Differences in the normalized levels of exogenous LDH across cell-laden hydrogels therefore indicate difference in the extent of cell death induced by various formulations. Although the exogenous LDH activity at 24 h was higher for the hydrogel containing 20 wt % **C** ($\mathbf{C_{20}H_{80}}$) versus the corresponding pure PEG-DA hydrogel (**H control**), the hydrogels containing 1 wt% ($\mathbf{C_1H_{99}}$) and 10 wt% ($\mathbf{C_{10}H_{90}}$) of **C** demonstrated similar cytocompatibility. At 72 h, $PDMS_{star}$-PEG hydrogels showed statistically similar levels of exogenous LDH activity whereas $C_{20}H_{80}$ was only slightly higher. Thus, $PDMS_{star}$-PEG hydrogels appear to maintain the low cytotoxicity of PEG-DA hydrogels over a range of PDMS levels.

In addition, $\mathbf{A_{10}H_{90}}$ hydrogels stained with the Live-Dead assay at 24 and 72 h post-encapsulation exhibited similar cell viability (~75%) as the **H control** (Figure 7). These two assessments indicate that $PDMS_{star}$-PEG hydrogels appear to maintain the low cytotoxicity of PEG-DA hydrogels. Since PEG hydrogels such as **H control** are considered non-cytotoxic, $PDMS_{star}$-PEG hydrogels appear to be non-cytotoxic as well.[49, 50]

NIH-PA Author Manuscript

NIH-PA Author Manuscript

NIH-PA Author Manuscript

Conclusion

A library of 18 unique $PDMS_{star}$-PEG hydrogels were formed by the rapid photocrosslinking of 10 wt% aqueous precursor solutions containing varying weight ratios (0:100, 1:99, 10:90 and 20:80, respectively) of $PDMS_{star}$-MA (**A–C**: 1.8k, 5k and 7k g/mol, respectively) and PEG-DA (**L** and **H**: 3.4k and 6k g/mol, respectively). PEG-DA hydrogels are single-component systems in which only two compositional variables (e.g. PEG-DA M_n and concentration) may be utilized to alter hydrogel properties. These $PDMS_{star}$-PEG hydrogels are two-component systems in which four compositional variables (e.g. PEG-DA and $PDMS_{star}$-MA M_n and concentration) may be altered to tune physical and additionally chemical properties. The chemical properties of the hydrogels were switched from a purely organic PEG to inorganic-organic with increased levels of **A–C**. Hydrogel morphology consisted of spherical PDMS-enriched microparticles dispersed throughout a PEG matrix. For hydrogels based on **L**, increased levels of **A–C** systematically decreased tensile modulus and a similar but less substantial decrease was observed for hydrogels based on **H**. At the same weight ratio, the Mn of **A–C** did not significantly impact mechanical properties. For a given hydrogel series based on **L** or **H**, the equilibrium swelling did not differ substantially across hydrogel formulations relative to that of the corresponding pure PEG-DA hydrogel (**L** and **H controls**). Thus, for a given hydrogel series, modulus was decoupled from equilibrium swelling. These hydrogels therefore would permit the evaluation of the effect of scaffold modulus on cell behavior apart from hydration. The resistance to non-specific protein adsorption, controlled introduction of bioactivity, and low cytotoxicity of PEG-DA hydrogels was maintained for the PDMSstar-PEG hydrogels. The non-degradability of these PDMSstar-PEG hydrogels will provide constant chemical and physical properties useful for controlled studies of cell-material interactions. However, as with pure PEG-DA hydrogels, these PDMSstar-PEG hydrogels may be rendered biodegradable by incorporation of enzymatically labile peptides[21, 22] or hydrolytically labile linear esters[23–25] to permit eventual replacement by the growing tissue. In future studies, $PDMS_{star}$-PEG hydrogels prepared with weight ratios higher than 20:80 ($PDMS_{star}$:PEG) will be similarly studied.

Supplementary Material

Refer to Web version on PubMed Central for supplementary material.

Acknowledgments

Funding from the NIH/NHLBI (1R21HL089964) is gratefully acknowledged.

References

1. Langer R, Vacanti JP. Tissue engineering. Science 1993;260:920–926. [PubMed: 8493529]
2. Liu C, Xia Z, Czernuszka JT. Design and development of three-dimensional scaffolds for tissue engineering. Chem Eng Res Design 2007;85:1051–1064.
3. Agrawal CM, Robert BR. Biodegradable polymeric scaffolds for musculoskeletal tissue engineering. J Biomed Mater Res 2001;55:141–150. [PubMed: 11255165]
4. Lavik E, Langer R. Tissue engineering: current state and perspectives. Appl Microbiol Biotechnol 2004;65:1–8. [PubMed: 15221227]
5. Drury JL, Mooney DJ. Hydrogels for tissue engineering: scaffold design variables and applications. Biomaterials 2003;24:4337–4351. [PubMed: 12922147]
6. Lee KY, Mooney DJ. Hydrogels for tissue engineering. Chem Rev 2001;101:1869–1879. [PubMed: 11710233]
7. Cushing MC, Anseth KS. Hydrogel cell cultures. Science 2007;316:1133–1134. [PubMed: 17525324]

NIH-PA Author Manuscript

NIH-PA Author Manuscript

NIH-PA Author Manuscript

8. Hoffman AS. Hydrogels for biomedical applications. Adv Drug Deliv Rev 2002;54:3–12. [PubMed: 11755703]
9. Peppas NA, Bures P, Leobandung W, Ichikawa H. Hydrogels in pharmaceutical formulations. Eur J Pharm Biopharm 2000;50:27–46. [PubMed: 10840191]
10. Ifkovits JL, Burdick JA. Review: Photopolymerizable and degradable biomaterials for tissue engineering applications. Tissue Eng 2007;13:2369–2385. [PubMed: 17658993]
11. Elisseeff J, Anseth K, Sims D, McIntosh W, Randolph M, Langer R. Transdermal photopolymerization for minimally invasive implantation. Proc Natl Acad Sci 1999;96:3104–3107. [PubMed: 10077644]
12. Burdick JA, Anseth KS. Photoencapsulation of osteoblasts in injectable RGD-modified PEG hydrogels for bone tissue engineering. Biomaterials 2002;23:4315–4323. [PubMed: 12219821]
13. Yang F, Williams CG, Wang DA, Lee H, Manson PN, Elisseeff J. The effect of incorporating RGD adhesive peptide in polyethylene glycol diacrylate hydrogel on osteogenesis of bone marrow stromal cells. Biomaterials 2005;26:5991–5998. [PubMed: 15878198]
14. Bryant SJ, Anseth KS. The effects of scaffold thickness on tissue engineered cartilage in photocrosslinked poly(ethylene oxide) hydrogels. Biomaterials 2001;22:619–626. [PubMed: 11219727]
15. Elisseeff J, McIntosh W, Anseth K, Riley S, Ragan P, Langer R. Photoencapsulation of chondrocytes in poly(ethylene oxide)-based semi-interpenetrating networks. J Biomed Mater Res 2000;51:164–171. [PubMed: 10825215]
16. Mahoney MJ, Anseth KS. Three-dimensional growth and function of neural tissue in degradable polyethylene glycol hydrogels. Biomaterials 2006;27:2265–2274. [PubMed: 16318872]
17. Kraehenbuehl TP, Ferreira LS, Zammaretti P, Hubbell JA. Cell-responsive hydrogel for encapsulation of vascular cells. Biomaterials 2009;30:4318–4324. [PubMed: 19500842]
18. Hahn MS, McHale MK, Wang E, Schmedlen RH, West JL. Physiological pulsatile flow bioreactor conditioning of poly(ethylene glycol)-based tissue engineering grafts. Ann Biomed Eng 2007;35:190–200. [PubMed: 17180465]
19. Gombotz WR, Guanghui W, Horbett TA, Hoffman AS. Protein adsorption to poly(ethylene oxide) surfaces. J Biomed Mater Res 1991;25:1547–1562. [PubMed: 1839026]
20. Hahn MS, Miller JS, West JL. Three-dimensional biochemical and biomechanical patterning for guiding cell behavior. Adv Mater 2006;18:2679–2684.
21. Halstenberg S, Panitch A, Rizzi S, Hall H, Hubbell JA. Biologically engineered protein-*graft*-poly (ethylene glycol) hydrogels: a cell adhesive and plasmin-degradable biosynthetic material for tissue repair. Biomacromolecules 2002;3:710–723. [PubMed: 12099815]
22. West JL, Hubbell JA. Polymeric biomaterials with degradation sites for proteases involved in cell migration. Macromolecules 1999;32:241–244.
23. Sawhney AS, Pathak CP, Hubbell JA. Bioerodible hydrogels based on photopolymerized poly (ethylene glycol)-*co*-poly(hydroxy acid) diacrylate macromers. Macromolecules 1993;26:581–587.
24. Martens PJ, Bryant SJ, Anseth KS. Tailoring the degradation of hydrogels formed from multivinyl poly(ethylene glycol) and poly(vinyl alcohol) macromers for cartilage tissue engineering. Biomacromolecules 2003;2003:283–292. [PubMed: 12625723]
25. Bryant SJ, Durand KL, Anseth KS. Manipulations in hydrogel chemistry control photoencapsulated chondrocyte behavior and their extracellular matrix production. J Biomed Mater Res 2003;67A: 1430–1436.
26. Kleinman HK, Philp D, Hoffman MP. The role of the extracellular matrix in morphogenesis. Curr Opin Biotechnol 2003;14:526–532. [PubMed: 14580584]
27. Lutolf MP, Hubbell JA. Synthetic biomaterials as instructive extracellular microenvironments for morphogensis in tissue engineering. Nature Biotech 2005;23:47–55.
28. Causa F, Netti PA, Ambrosio L. A multi-functional scaffold for tissue regeneration: The need to engineer a tissue analogue. Biomaterials 2007;28:5093–5099. [PubMed: 17675151]
29. Dado D, Levenberg S. Cell-scaffold mechanical interplay within engineered tissues. Sem Cell Dev Biol 2009;20:656–664.

NIH-PA Author Manuscript

NIH-PA Author Manuscript

NIH-PA Author Manuscript

30. Dutta RC, Dutta AK. Cell-interactive 3D-scaffold; advances and applications. Biotech Adv 2009;27:334–339.
31. Kim BS, Nikolovski J, Bonadio J, Smiley E, Mooney DJ. Engineered smooth muscle tissues: regulating cell phenotype with the scaffold. Exp Cell Res 1999;251:321–328.
32. Benoit DSW, Schwartz MP, Durney AR, Anseth KS. Small functional groups for controlled differentiation of hydrogel-encapsulated human mesenchymal stem cells. Nature Mater 2008;7:816–823. [PubMed: 18724374]
33. Escobar-Ivirico JL, Salmeron-Sanchez M, Gomez-Ribelles JL, Monleon-Pradas M, Soria JM, Gomes ME, Reis RL, Mano JF. Proliferation and differentiation of goat bone marrow stromal cells in 3D scaffolds with tunable hydrophilicity. J Biomed Mater Res 2009;91B:277–286.
34. Lin NJ, Lin-Gibson S. Osteoblast response to dimethacrylate composites varying in composition, conversion and roughness using a combinatorial approach. Biomaterials 2009;30:4480–4487. [PubMed: 19520423]
35. Song JH, Yoon BH, Kim YE, Kim HW. Bioactive and degradable hybridized nanofibers of gelatin-siloxane for bone regeneration. J Biomed Mater Res 2008;84:875.
36. Ning CQ, Mehta J, El-Ghannam A. Effect of silica on the bioactivity of calcium phosphate composites *in vitro*. J Mater Sci Mater Med 2005;16:355–360. [PubMed: 15803281]
37. Crouch AS, Miller D, Luebke KJ, Hu W. Correlation of anisotropic cell behaviors with topographic aspect ratio. Biomaterials 2009;30:1560–1567. [PubMed: 19118891]
38. Glawe JD, Hill JB, Mills DK, McShane MJ. Influence of channel width on alignment of smooth muscle cells by high-aspect-ratio microfabricated elastomeric cell culture scaffolds. J Biomed Mater Res 2005;75A:106–114.
39. Khetan S, Katz JS, Burdick JA. Sequential crosslinking to control cellular spreading in 3-dimensional hydrogels. Soft Matter 2009;5:1601–1606.
40. Engler AJ, Sen S, Sweeney HL, Discher DE. Matrix elasticity directs stem cell lineage specification. Cell 2006;126:677–689. [PubMed: 16923388]
41. Discher DE, Janmey P, Wang Y-l. Tissue cells feel and respond to the stiffness of their substrate. Science 2005;310:1139–1143. [PubMed: 16293750]
42. Liao H, Munoz-Pinto D, Qu X, Hou Y, Grunlan MA, Hahn MS. Influence of hydrogel mechanical properties and mesh size on vocal fold fibroblast extracellular matrix production and phenotype. Acta Biomaterialia 2008;4:1161–1171. [PubMed: 18515199]
43. Bryant SJ, Anseth KS. Hydrogel properties influence ECM production by chondrocytes photoencapsulated in poly(ethylene glycol) hydrogels. J Biomed Mater Res 2002;59:63–72. [PubMed: 11745538]
44. Munoz-Pinto DJ, Bulick AS, Hahn MS. Uncoupled investigation of scaffold modulus and mesh size on smooth muscle cell behavior. J Biomed Mater Res Part A 2009;90A:303–316.
45. Van-Dyke, ME.; Clarson, SJ.; Arshady, R. Silicone Biomaterials. In: Arshady, R., editor. Introduction to Polymeric Biomaterials. Vol. 1. Citus Books; London: 2003. p. 109-135.
46. Grunlan MA, Lee NS, Mansfeld F, Kus E, Finlay JA, Callow JA, Callow ME, Weber WP. Minimally adhesive polymer surfaces prepared from star oligosiloxanes and star oligofluorosiloxanes. J Polym Sci Part A: Polymer Chem 2006;44:2551–2566.
47. Boutevin B, Guida-Pietrasanta F, Ratsimihety A. Synthesis of photocrosslinkable fluorinated polydimethylsiloxanes: direct introduction of acrylic pendant groups via hydrosilylation. J Polym Sci Part A: Polym Chem 2000;38:3722–3728.
48. Hahn MS, Taite LJ, Moon JJ, Rowland MC, Ruffino KA, West JL. Photolithographic patterning of polyethylene glycol hydrogels. Biomaterials 2006;27:2519–2524. [PubMed: 16375965]
49. Williams CG, Malik AN, Kim TK, Manson PN, Elisseeff JH. Variable cytocompatibility of six cell lines with photoinitiators use for polymerizing hydrogels and cell encapsulation. Biomaterials 2005;26:1211–1218. [PubMed: 15475050]
50. Bryant SJ, Nuttelman CR, Anseth KS. Cytocompatibility of UV and visible light photoinitiating systems on cultured NIH/3T3 fibroblasts *in vitro*. J Biomater Sci Polym Ed 2000;11:439–457. [PubMed: 10896041]
51. Liu VA, Bhatia SN. Three-dimensional photopatterning of hydrogels containing living cells. Biomed Microdevices 2002;4:257–266.

NIH-PA Author Manuscript

NIH-PA Author Manuscript

NIH-PA Author Manuscript

52. Chojnowske, J. Polymerization. In: Clarson, SJ.; Semlyen, JA., editors. Siloxane Polymers. PTR Prentice Hall; Englewood Cliffs, JJ: 1993. p. 19-22.

53. Ford MC, Bertram JP, Hynes SR, Michaud M, Li Q, Young M, Segal SS, Madri JA, Lavik EB. A macroporous hydrogel for the coculture of neural progenitor and endothelial cells to form functional vascular networks *in vivo*. Proc Natl Acad Sci 2006;103:2512–2517. [PubMed: 16473951]

54. Hou Y, Matthews AR, Smitherman AM, Bulick AS, Hahn MS, Hou H, Han A, Grunlan MA. Thermoresponsive nanocomposite hydrogels with cell-releasing behavior. Biomaterials 2008;29:3175–3184. [PubMed: 18455788]

55. Ren L, Tsuru K, Hayakawa S, Osaka A. Novel approach to fabricate porous gelatin-siloxane hybrids for bone tissue engineering. Biomaterials 2002;23:4765–4773. [PubMed: 12361615]

56. Anseth KS, Bowman CN, Brannon-Peppas L. Mechanical properties of hydrogels and their experimental determination. Biomaterials 1996;17:1647–1657. [PubMed: 8866026]

57. Mann BK, Gobin AS, Tsai AT, Schmeldlen RH, West JL. Smooth muscle cell growth in photopolymerized hydrogels with cell adhesive and proteolytically degradable domains: synthetic ECM analogs for tissue engineering. Biomaterials 2001;22:3045–3051. [PubMed: 11575479]

58. Ju H, McCloskey BD, Sagle AC, Kusuma VA, Freeman BD. Preparation and characterization of crosslinked poly(ethylene glycol) diacrylate hydrogels as fouling-resistant membrane coatings. J Mem Sci 2009;330:180–188.

59. Anderson JM, Ziats NP, Azeez A, Brunstedt MR, Stack S, Bonfield TL. Protein adsorption and macrophage activation on polydimethylsiloxane and silicone rubber. J Biomater Sci Polym Ed 1995;7:159–169. [PubMed: 7654630]

60. Renner K, Amberger A, Konwalinka G, Kofler R, Gnaiger E. Changes of mitochondrial respiration, mitochondrial content and cell size after induction of apoptosis in leukemia cells. Biochim Biophys Acta 2003;1642:115–123. [PubMed: 12972300]

NIH-PA Author Manuscript

NIH-PA Author Manuscript

NIH-PA Author Manuscript

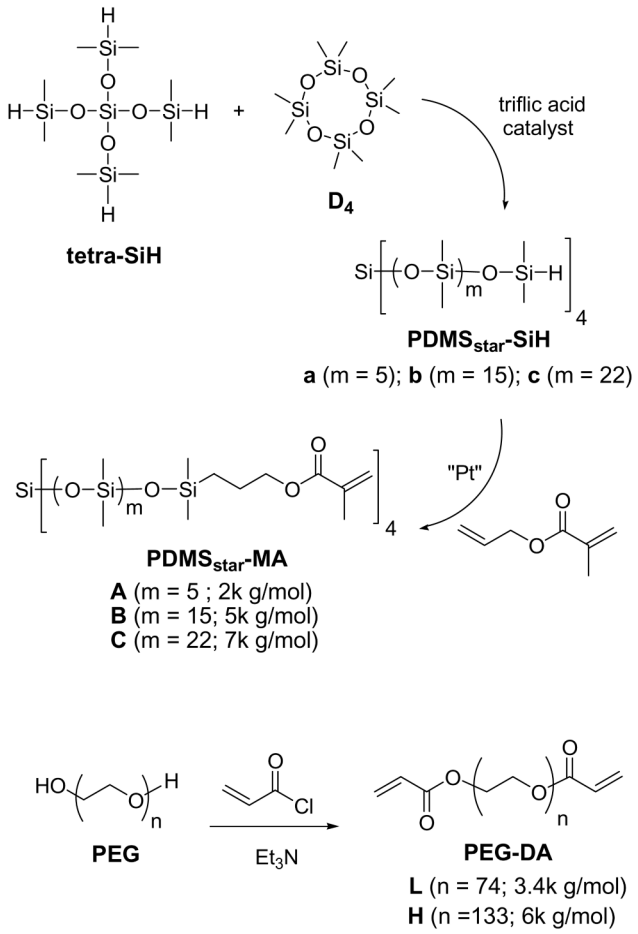

Figure 1.

Synthesis of (top) inorganic $PDMS_{star}$-MA (**A–C**) macromonomers and (bottom) organic PEG-DA (**L, H**) macromonomers.

NIH-PA Author Manuscript

NIH-PA Author Manuscript

NIH-PA Author Manuscript

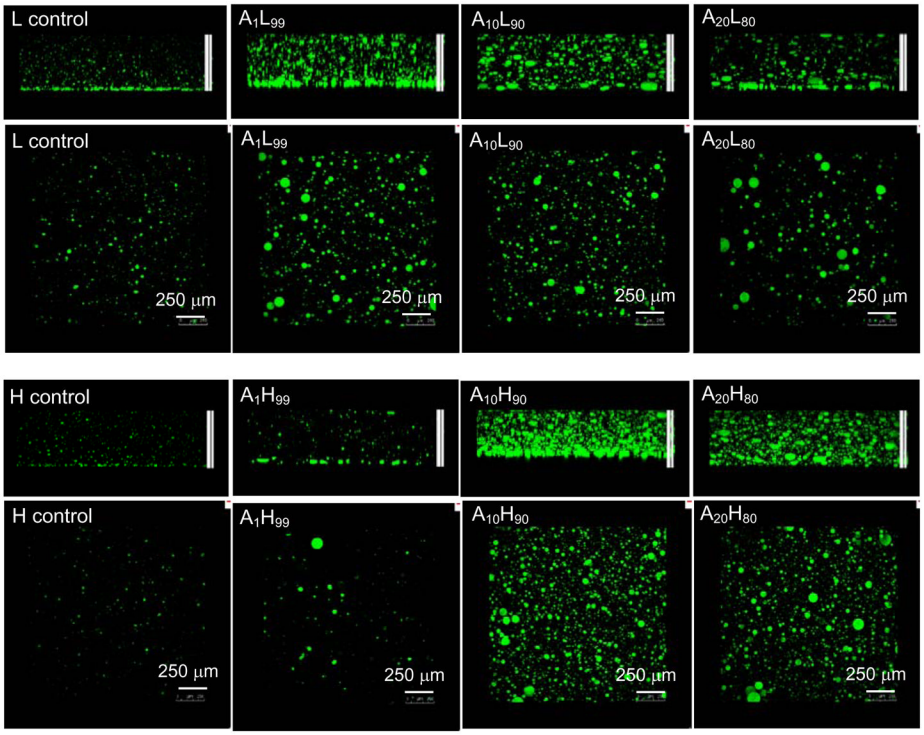

Figure 2.
CLSM images of hydrated hydrogels stained with Nile Red. Cross-sectional view (top rows) and top view (bottom rows). The hydrophobic dye stained hydrophobic PDMS-enriched microparticles.

NIH-PA Author Manuscript

NIH-PA Author Manuscript

NIH-PA Author Manuscript

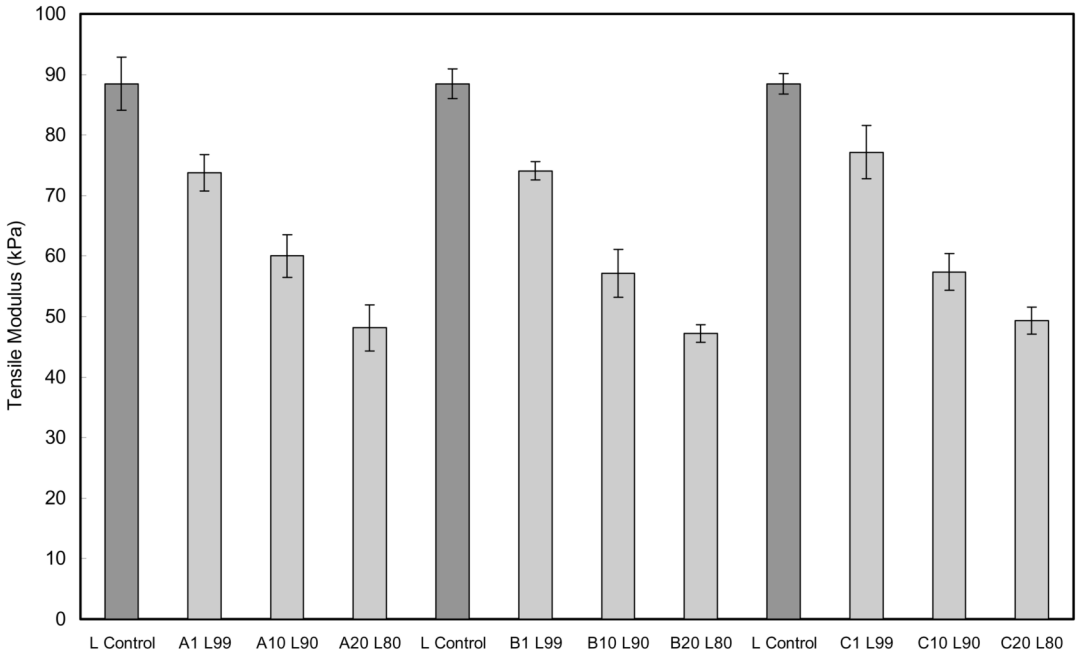

Figure 3.

Tensile modulus of hydrogels based on **L**. Statistical significance within a given series (i.e. A, B and C) was determined by one-way analysis of variance (Holm-Sidak method where $p \leq 0.05$.) For a given series, all are statistically different versus the control and other compositions.

NIH-PA Author Manuscript

NIH-PA Author Manuscript

NIH-PA Author Manuscript

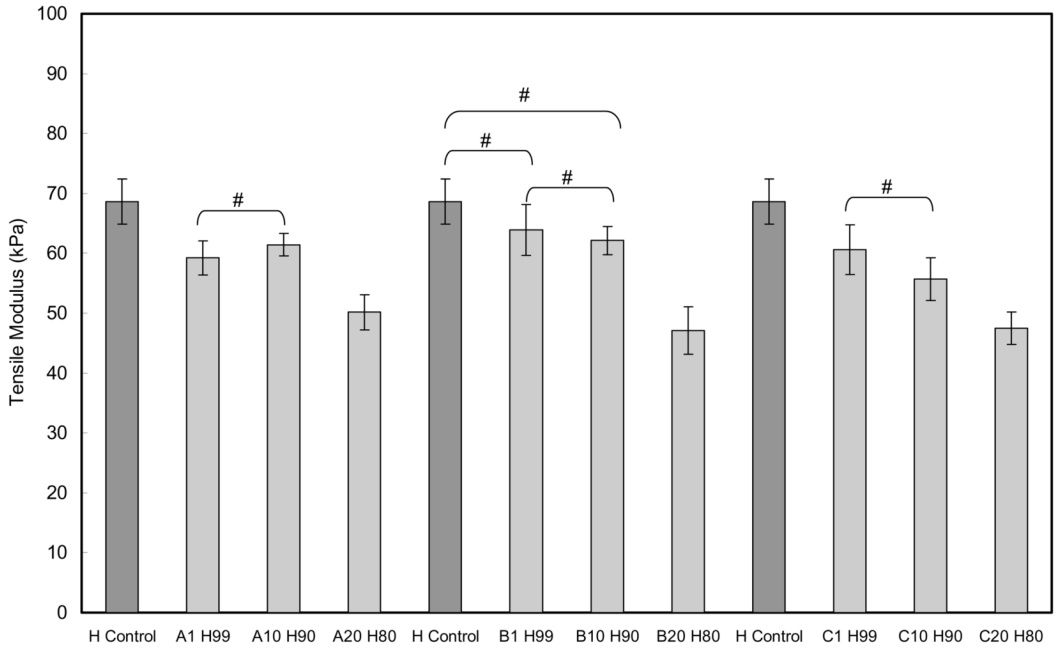

Figure 4.

Tensile modulus of hydrogels based on **H**. Statistical significance within a given series (i.e. **A**, **B** and **C**) was determined by one-way analysis of variance (Holm-Sidak method where $p \leq 0.05$, unless otherwise noted. [#] indicates $p > 0.05$).

NIH-PA Author Manuscript
NIH-PA Author Manuscript
NIH-PA Author Manuscript

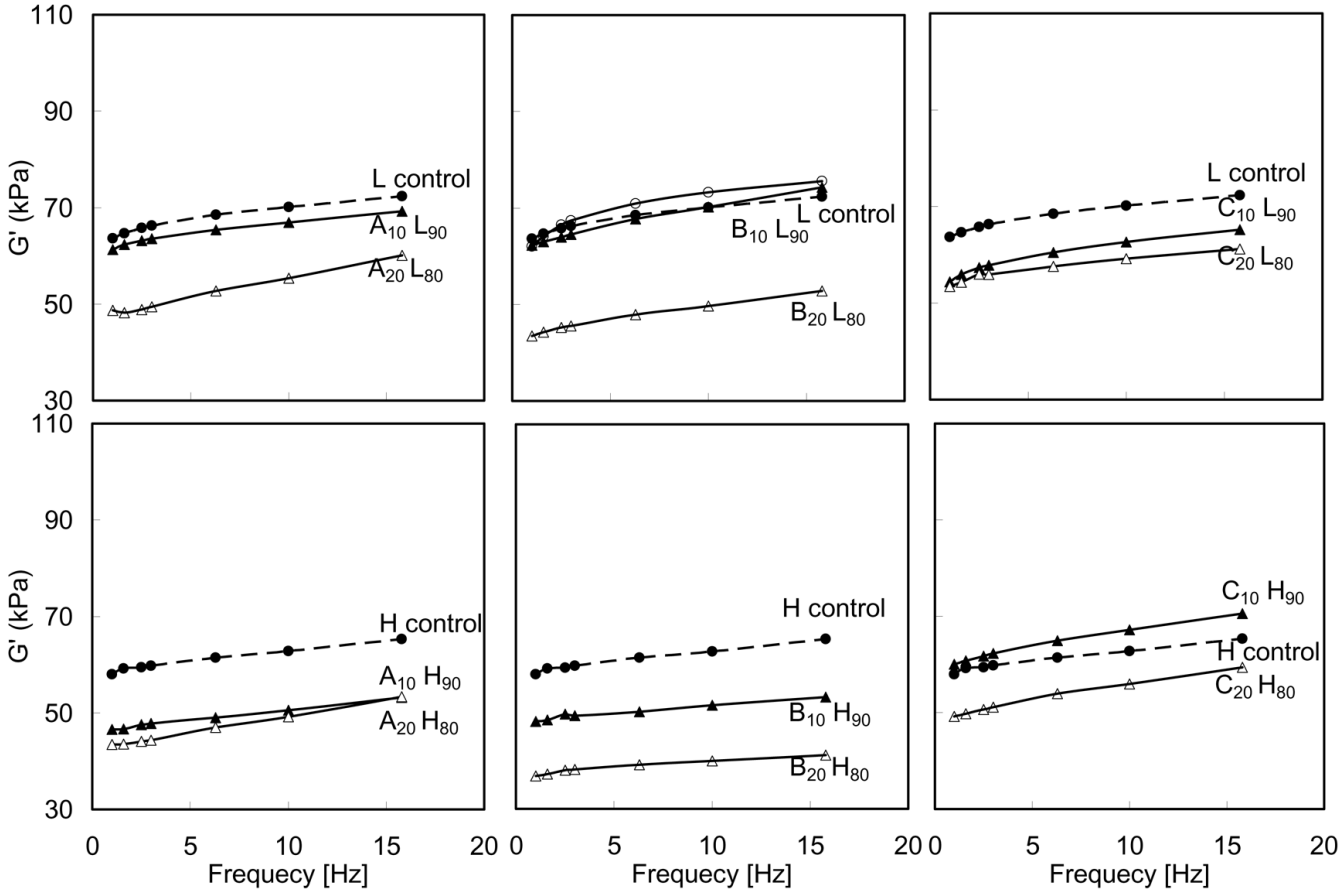

Figure 5.
Storage modulus (G') of hydrogels measured in compression.

NIH-PA Author Manuscript
NIH-PA Author Manuscript
NIH-PA Author Manuscript

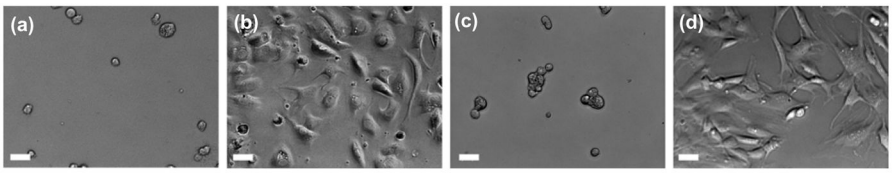

Figure 6.
Cell spreading is not observed for both (a) H control prepared without RGDS (cell-adhesive peptide) and **(c) $A_{10}H_{90}$** prepared without RGDS. Cell spreading is observed on (b) H control prepared with RGDS **a**nd **(d) $A_{10}H_{90}$** prepared with RGDS. Scale bars = 100 μm.

NIH-PA Author Manuscript

NIH-PA Author Manuscript

NIH-PA Author Manuscript

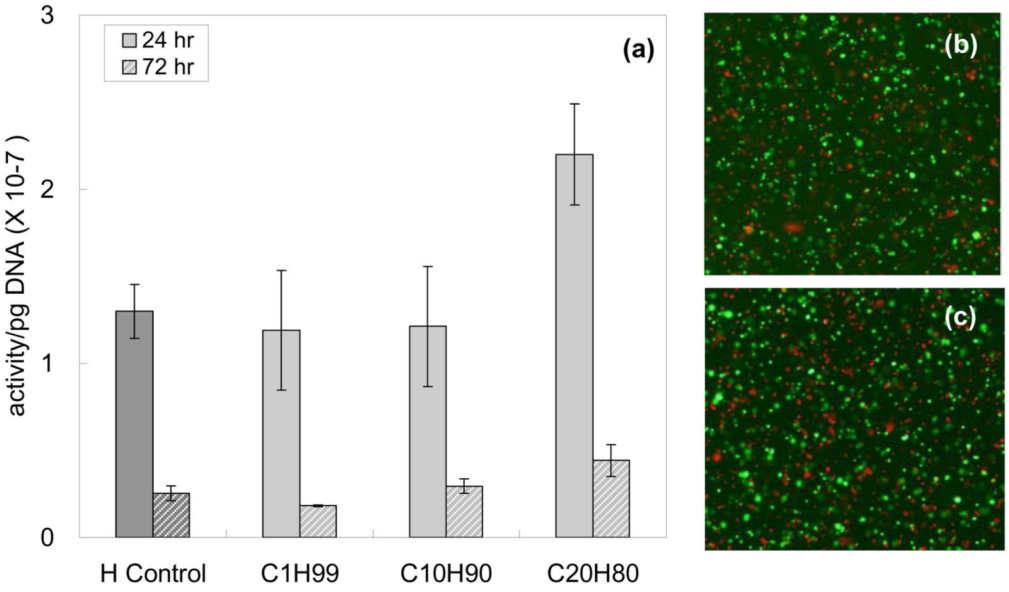

Figure 7.

(a) LDH activity at 24h (left columns) and 72 h (right columns). Representative fluorescent image of Live-Dead stained hydrogels **(b) H control** and **(c) $A_{10}H_{90}$**. Live (green) cells constitute ~75% of both.

NIH-PA Author Manuscript

NIH-PA Author Manuscript

NIH-PA Author Manuscript

Table 1

Hydrogel Composition and Notation

	PDMS$_{star}$-MA			
PEG-DA	**Wt% ratio: A–C: L**	**A M_n = 2k g/mol**	**B M_n = 5k g/mol**	**C M_n = 7k g/mol**
L	0:100		**L control**	
M_n = 3.4k	1:99	**A_1 L99**	**B_1 L 99**	**C_1 L $_{99}$**
g/mol	10:90	**A_{10} L 90**	**B_{10} L 90**	**C_{10} L $_{90}$**
	20:80	**A_{20} L 80**	**B_{20} L 80**	**C_{20} L $_{80}$**

	PDMS$_{star}$-MA			
PEG-DA	**Wt% ratio: A–C: H**	**A M_n = 2k g/mol**	**B M_n = 5k g/mol**	**C M_n = 7k g/mol**
H	0:100		**H control**	
M_n = 6k	1:99	**A_1 H_{99}**	**B_1 H $_{99}$**	**C_1 H $_{99}$**
g/mol	10:90	**A_{10} H $_{90}$**	**B_{10} H $_{90}$**	**C_{10} H $_{90}$**
	20:80	**A_{20} H $_{80}$**	**B_{20} H $_{80}$**	**C_{20} H $_{80}$**

NIH-PA Author Manuscript NIH-PA Author Manuscript NIH-PA Author Manuscript

Table 2

Hydrogel swelling ratio, tensile strength (TS), % elongation at break (%EL), and adsorption of BSA protein.

	Swelling Ratio	Tensile Strength (kPa)	% EL	mg BSA adsorbed per cm^2 ($\times 10^{-4}$)*
L control	**7.0 ± 0.01**	**34.2 ± 3.0**	**40.5 ± 4.0**	**5.2 ± 1.2**
A_1 L_{99}	6.5 ± 0.03	34.5 ± 4.2	49.2 ± 4.9	3.6 ± 0.6
A_{10} L $_{90}$	6.2 ± 0.04	27.5 ± 3.4	48.5 ± 4.1	13.5 ± 3.5
A_{20} L $_{80}$	6.7 ± 0.05	22.3 ± 2.9	49.2 ± 7.2	25.7 ± 4.9
B_1 L $_{99}$	6.6 ± 0.15	34.4 ± 5.2	48.8 ± 7.0	9.4 ± 1.7
B_{10} L $_{90}$	6.6 ± 0.12	26.0 ± 2.9	48.2 ± 5.0	14.5 ± 1.5
B_{20} L $_{80}$	7.1 ± 0.10	20.0 ± 2.7	45.2 ± 4.9	28.7 ± 6.4
C_1 L $_{99}$	6.7 ± 0.14	40.6 ± 9.4	55.0 ± 9.0	14.1 ± 6.4
C_{10} L $_{90}$	6.8 ± 0.05	29.0 ± 3.5	53.6 ± 6.3	5.7 ± 2.6
C_{20} L $_{80}$	7.3 ± 0.08	24.5 ± 1.8	53.4 ± 4.4	19.0 ± 1.6
H control	**8.0 ± 0.06**	**39.7 ± 7.7**	**61.0 ± 9.3**	**12.4 ± 4.7**
A_1 H_{99}	8.0 ± 0.06	35.5 ± 2.4	64.0 ± 3.3	10.1 ± 1.8
A_{10} H $_{90}$	8.0 ± 0.11	48.1 ± 5.0	82.9 ± 7.4	16.0 ± 4.3
A_{20} H $_{80}$	7.9 ± 0.11	37.1 ± 6.7	77.4 ± 9.9	10.2 ± 1.9
B_1 H $_{99}$	8.0 ± 0.18	39.7 ± 5.3	65.9 ± 5.4	5.3 ± 2.1
B_{10} H $_{90}$	8.1 ± 0.09	46.0 ± 4.3	79.2 ± 4.8	15.0 ± 9.9
B_{20} H $_{80}$	8.1 ± 0.08	26.8 ± 6.8	59.6 ± 10.8	8.6 ± 1.1
C_1 H $_{99}$	8.0 ± 0.01	33.4 ± 5.9	58.5 ± 6.5	15.0 ± 1.6
C_{10} H $_{90}$	8.1 ± 0.23	25.6 ± 4.3	51.1 ± 5.1	12.8 ± 3.1
C_{20} H $_{80}$	8.4 ± 0.16	33.6 ± 4.5	73.6 ± 6.2	10.0 ± 1.3

*After 3 hr exposure to BSA (0.1 mg/mL PBS)